COMMON CHARACTERISTICS OF CMES AND BLOBS: A NEW VIEW OF THEIR POSSIBLE ORIGIN

V. G. ESELEVICH and M. V. ESELEVICH
Institute of Solar-Terrestrial Physics, P.O. Box 4026, 664033 Irkutsk 33, Russia
(e-mail: esel@iszf.irk.ru)

(Received 26 February 2001; accepted 12 June 2001)

Abstract. An analysis of the LASCO/SOHO data has shown that blobs are similar, in their basic characteristics, to CMEs, having a relatively small size and relatively low velocities. The formation of blobs and CMEs is usually accompanied by the process where a separate ray (or rays) of the streamer belt becomes occupied by additional anti-sunward traveling plasma of increased density. Generally the size of a CME in the plane of the streamer belt can exceed the CME size in the direction normal to the belt. Conceivably the formation mechanism of CMEs and their energetics might be associated with the energy of additional anti-sunward traveling plasma. This should be taken into account when constructing theoretical models of CMEs.

1. Introduction

Investigations of the origin of the streamer belt using the LASCO/SOHO instruments revealed the existence of small-scale (about $0.1R_\odot$ in transverse size, where $R_\odot$ is the solar radius) plasma density inhomogeneities (blobs) traveling in the anti-sunward direction (Sheeley *et al.*, 1997). As pointed out by Wang *et al.* (1998), blobs are continually emitted from the elongated tips of helmet streamers at $3-4\ R_\odot$ from the Sun's center, and propagate within a thin plasma layer that surrounds the heliospheric current sheet of the streamer belt. It was suggested (Wang *et al.*, 1998) that both the blobs and the plasma sheet can result from a partial decay of streamers in the region of the helmet tops, presumably due to the process of magnetic field-line reconnection. Further studies by Eselevich and Eselevich (1999, hereinafter referred to as Paper 1) at large distances $R > 3-4\ R_\odot$ showed that in the absence of coronal mass ejections (CMEs), the streamer belt represents a sequence of radial rays of increased brightness. The smallest possible size d of a ray is $\approx 2-3$ deg. The rays sustain both a quasi-stationary solar wind (SW) whose parameters vary relatively slowly with a typical time of up to 10 days or longer (Eselevich and Eselevich, 2000a), and sporadic (non-stationary) plasma motions with a typical lifetime of about several hours. The latter type includes: (a) the above-mentioned inhomogeneities of material traveling in the anti-sunward direction (blobs); and (b) the recently discovered sporadic plasma flows directed both anti-sunward and sunward (Wang *et al.*, 1999a, b). The non-stationary SW should also include the formation stage of a quasi-stationary SW observed in some cases

Solar Physics **203:** 165–178, 2001.

when an additional anti-sunward traveling plasma of increased density occupies a separate ray (Eselevich and Eselevich, 2000a).

This paper aims at identifying which characteristics are shared by such sporadic processes in the streamer belt as the occupation of the ray by an additional anti-sunward traveling plasma of increased density, blobs, and CMEs.

2. Identification of Rays in the Streamer Belt – Method of Analysis

The study reported in this paper was carried out on the basis of the white-light corona brightness data from the LASCO C2 and C3 instruments aboard the SOHO spacecraft which are available through the Internet. The C2 and C3 coronagraphs provide white-light corona images within $R = 2–6\ R_\odot$ and $R = 3.7–30\ R_\odot$, respectively. Daily images in the mpeg format were used in the study. Each mpeg file contains a series of solar corona images throughout a single day. The procedure of deriving experimental information from white-light corona images involved the following steps. Individual images corresponding to particular times were extracted from the mpeg files. Data contained in these images were used to construct corona brightness distributions $P(\Lambda)$ at different distances R from the Sun's center, separately for the E or W limbs, or the $P(R)$ distribution at fixed Λ. Here Λ is the apparent (in the plane of the sky) latitude of the streamer belt's ray or the angle between the apparent image of the ray in the plane of the sky and the equatorial plane. Λ is positive and negative to the north and south of the equator, respectively. Values of the brightness P are measured in arbitrary units, and lie in the range from 0 to 255. The resulting distributions were used to infer $P(\Lambda)$, the ray brightness P_R, the definition of which was given in Paper 1. The possibility of introducing the notion of the ray brightness P_R is due to the fact that the ray is distinguished on the brightness profile $P(\Lambda)$ by the slope of the two lines forming it, which from the top P_M, a maximum ray brightness, to the inflection points A and B, may be represented as straight lines. This permits us to introduce a definition of the ray brightness $P_R = P_M - P_B$ and of the angular size d, as shown in the bottom panel of Figure 1, where P_B is the background brightness.

3. Comparative Analysis of CMEs and Blobs

Since blobs are produced and propagate (as shown in Paper 1) within separate rays of the streamer belt, the selection of the orientation of the plane of the streamer belt with respect to the plane of the sky is of significant importance when investigating them.

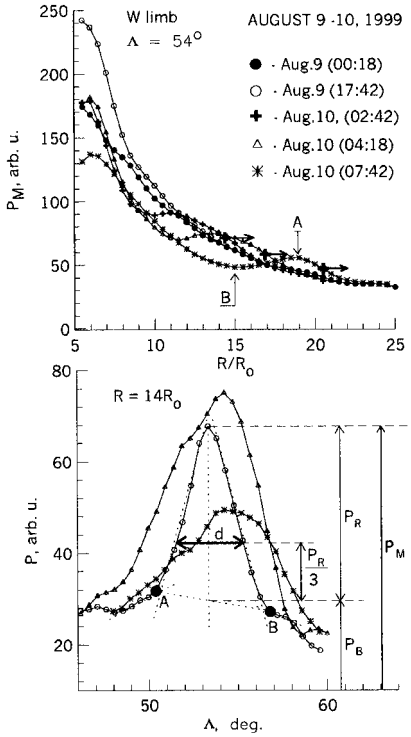

Figure 1. Brightness distribution in the case of the generation and propagation of a blob within the brightness ray of the streamer belt at the W limb and at $\Lambda \approx 54^\circ$ at different times depending (*upper panel*) on the normalized distance from the Sun's center, and (*bottom panel*) on the apparent latitude at $R = 14\ R_\odot$, 9–10 August 1999. Streamer belt in the plane of the sky.

3.1. THE STREAMER BELT IN THE PLANE OF THE SKY

Let us consider the situation where the streamer belt lies in the plane of the sky. In this case, all observed changes in ray brightness, during 24 hours at least, are the manifestation of actual sporadic processes occurring in the ray. Figure 1 (upper panel) and Figure 2 (upper panel) show the distributions of maximum brightness P_M as a function of the normalized distance $R/R_\odot$ from the Sun's center along the selected ray, respectively, for the blob (9–10 August 1999, W limb, $\Lambda \approx 54^\circ$ (northern hemisphere)), and for a small CME (20 October 1999, E limb, $\Lambda \approx -18^\circ$ (southern hemisphere)).

From the position of the calculated neutral line which is known to run along the streamer belt, it is easy to see that in the events under consideration the streamer belt lies virtually in the plane of the sky. Two processes are rather clearly identifiable in the formation and propagation pattern of the blob in Figure 1 (upper panel). One of the them is taking place at successive times between 00:18 UT (filled circle) and 17:42 UT (open circle) on 9 August 1999, and manifests itself as an increase in plasma brightness (density) associated with the occupation of the ray

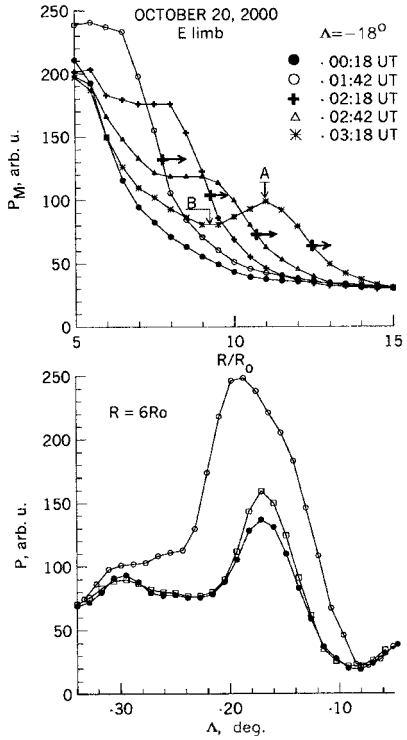

Figure 2. Brightness distribution in the case of the generation and propagation of small CME within the brightness ray of the streamer belt at the W limb and at $\Lambda \approx -18^\circ$ at different times depending (*upper panel*) on the normalized distance from the Sun's center; and (*bottom panel*) on the apparent latitude at $R = 6\ R_\odot$, 20 October 1999. Streamer belt in the plane of the sky.

by an additional plasma from the Sun (or a higher density plasma which is fed into the ray). The velocity of the plasma front with such an occupation at $R \approx 7\ R_\odot$ is typically 80–100 km s^{-1}, i.e., about the velocity of the main quasi-stationary wind flowing within the ray prior to this occupation (Eselevich and Eselevich 2000b). This velocity is estimated from maximum brightness $P_M(R)$ as a function of the normalized distance (constructed with higher than in Figure 1 spatial resolution, at successive times between 00:18 UT and 17:42 UT on 9 August 1999, as done in Eselevich and Eselevich (2000b). The other process that is occurring when the ray becomes occupied by a new plasma flow involves the formation of a blob which is characterized by the appearance and anti-sunward propagation of a density hump (maximum A in Figure 1, upper panel), and by the following decrease in density (minimum B). By analogy with CMEs, we call them, respectively, the forward region of compression, and the cavity of the blob. Our analysis of several events showed that such a structure is characteristic of blobs.

The two processes considered above for blobs occur also during the formation of a small CME. Indeed, it is evident from Figure 2 (upper panel) that prior to

about 01:42 UT, the ray is occupied by plasma with higher density, followed by the appearance of two typical signatures of a propagating CME: the forward region of compression with a maximum at the point A, and the cavity with a minimum at the point B. It is difficult to say at present where the ultimate formation of this CME occurs: near the solar surface, during the anti-sunward propagation or at the point of observation. However, this event corresponds – in its morphological signatures at $R > 5$–$10\ R_\odot$ – to a typical CME of a small size. An important common signature of the two events under consideration (the blob, and the CME) is the increase $D = d - d_0$ of the initial angular size of the ray d_0, within which they propagate. As is apparent from Figure 1 (bottom panel) the value of D in the region of the cavity (10 August, 07:42 UT at $R = 14\ R_\odot$) can be as large as 100% or more of the original ray size $d = d_0$. Note that in the cavity region at the point B the value of $P_R = P_M - P_B > 0$, i.e., the ray persists, but this value is smaller than that of P_R at the point A in the compression region. An increase of angular size of the ray D with time (smaller in magnitude compared with the case of the blob and the CME) occurs also when the ray is occupied by additional plasma from the Sun.

To illustrate more clearly the role played by additional plasma from the Sun occupying the rays during the formation of a CME, let us consider the situation at the E limb during 5 November and at the beginning of 6 November 1999 (Figure 3). During this time interval, the streamer belt lay virtually in the plane of the sky. At the end of 5 November, there occurred a powerful CME which propagated along the streamer belt. Figure 3 (bottom panel) presents the brightness distributions $P(\Lambda)$ at three times on 5 November 1999, at the E limb and at $R = 7\ R_\odot$. It is evident from the figure that prior to the appearance of the CME within $\Lambda \approx -10°$ and $+60°$, there are four pronounced maxima of P corresponding to radial brightness rays A, B, C and D of the streamer belt (filled circles, 16:19 UT). Prior to the arrival of CMEs at $R = 7\ R_\odot$ at 19:43 UT, the greatest brightness enhancements ($> 20\%$) occur in rays B and C, whereas the brightness between these rays (at $\Lambda \approx 30°$) remains unchanged to within $\Delta P/P \approx \pm 5\%$. It is interesting to note that at $R = 5.5\ R_\odot$ (the respective figure is not reproduced here) the enhancements in rays A, B, C and D reach 100% or more, while the brightness between them remains unchanging to within $\Delta P/P \approx \pm 5\%$. These enhancements of P suggest that the rays are occupied by plasma of increased density. Later, at 21:42 UT, the brightness is somewhat enhanced throughout the latitude range $\Lambda \approx -10°$ and $+60°$, however, separate conspicuous rays are still identifiable as well as the inhomogeneity of the leading edge of CME density. A small brightness peak at about -12 deg is not a ray because at distances larger than $10\ R_\odot$ it is absent. The $P(R)$-distributions in rays B and C on 6 November at 05:17 UT are shown in Figure 3 (upper panel) by dark and open circles, respectively. They differ both by the form of the P-profiles and by the velocity of there leading edges. The amplitude h of the front is shown by the lower curve in Figure 3 (upper panel). The middle points of the fronts at the height $h/2$ are shown by a cross with the arrow pointed toward the direction of motion.

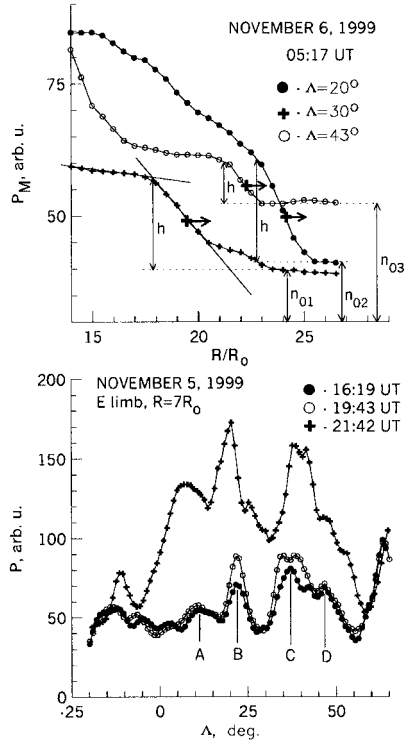

Figure 3. Brightness distribution in the case of the propagation of the CME with the angular opening including several rays of increased brightness, along the streamer belt lying in the plane of the sky at the E limb depending (*upper panel*) on the normalized distance from the Sun's center for three values of the apparent latitude (*filled circle* – $\Lambda = 20°$, *plus* – $\Lambda = 30°$, and *open circle* – $\Lambda = 43°$) on 6 November 1999 at 05:17 UT; and (*bottom panel*) on the apparent latitude Λ at $R = 7\ R_\odot$ on November 5, 1999, at three times (*filled circle* – 16:19 UT, *open circle* – 19:43 UT, and *plus* – 21:42 UT).

The front of the radial brightness distribution at the latitude $\Lambda = 30°$ between rays *B* and *C* (*pluses* in Figure 3 upper panel) is markedly delayed with respect to the fronts of rays *B* and *C*. These phenomena may be interpreted as follows: the formation process of the CME is accompanied by the occupation of one or several brightness rays by additional plasma with increased density (pressure), followed by a rapid 'blowing' (expansion) of these rays in the transverse direction, and by the formation of a single CME body.

Also, it follows from what has been said above that the angular size of the CME in the plane of the streamer belt must depend on the number of expanding rays which form this CME. In the event under consideration, the number of such rays is three or four (four rays *A*, *B*, *C* and *D* correspond to the angular opening of the CME, but not all of them expand and, accordingly, contribute to the production of the CME).

By analogy with the value (determined above) of D for a blob propagating in an individual ray, for the events under consideration we introduce a quantity D which represents the average increase in angular size of the rays constituting the CME body (i.e., over the angular size of the CME along the streamer belt),

$$D = \frac{1}{n}\sum_{i=1}^{n}(d_i - d_0), \tag{1}$$

where n is the number of expanding rays observed at the full angular opening of the CME; d_i is the angular size of the ith expanded ray; and d_0 is the initial angular size of the ray prior to its expansion. (For all rays, the value of d_0 is taken to be the same and equal to $d_0 = 3°$). In the CME under consideration, for $n = 3$–4 we have $D = 12°$–$17°$.

3.2. THE STREAMER BELT IS NORMAL TO THE PLANE OF THE SKY

The propagation of a CME along the streamer belt when the belt is normal (or nearly normal) to the plane of the sky is of interest because the smallest observed angular size of the CME can be expected in such events. The reason is that with such an orientation of the belt with respect to the plane of the sky, the sequence of rays of increased brightness forming the belt lines up along the line of sight, and merge into a single ray for the ground-based observer (Eselevich and Eselevich, 2000b). The angular size of the CME in such observations will, therefore, be determined by the angular expansion of one ray only. Eselevich and Eselevich (2000b) showed that within distances R from the Sun's center smaller than the height of the streamer helmet ($R < 2$–$3\ R_\odot$), any pair of neighboring rays oppositely bend towards the streamer helmet. Also, the minimum angular size of the rays $\approx 2°$–$3°$ remains virtually constant within $R = 1.2$–$6.0\ R_\odot$. Note that all of the events under investigation consist (within the measuring accuracy) of only two rays lying left and right of the streamer belt. Our recent investigations have shown, however, that the merging of the rays bending towards the helmet at distances $R > 2$–$3\ R_\odot$ above the helmet top does not always occur. In some events where the streamer belt is perpendicular to the plane of the sky, two closely-spaced rays (with the distance between the rays on the order of the ray diameter) can be observed at $R > 2$–$3\ R_\odot$. That is, in these cases the streamer belt consists of pairs of closely-spaced brightness rays. Such (or similar) a situation occurred prior to the production of the CME in the following events chosen for the analysis: 23 December 1996 (W limb); 13–14 August 1997 (W limb); 4 November 1997 (E limb); and 1–2 June 1998 (W limb). In spite of some differences, all of them shared the property of additional anti-sunward plasma inside the rays. We now carry out a detailed analysis of these features by considering one of the events, 4 November 1997. A segment of the 11 November 1997 NL, elongated along the parallel, near the southern latitude S13 ($\Lambda = -13°$), corresponds to the portion of the streamer belt on the synoptic map of Carrington rotation CR 1929 observed on 4 November 1997, at the E limb.

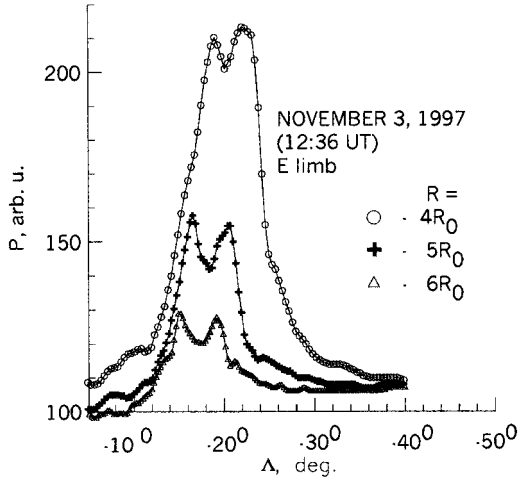

Figure 4. Brightness distribution P as a function of the apparent latitude in the case of a streamer belt perpendicular to the plane of the sky, at different distances R from the Sun's center: ○, $R = 4\ R_\odot$, +, $R = 5\ R_\odot$, and △, $R = 6\ R_\odot$. 3 November 1997, E limb.

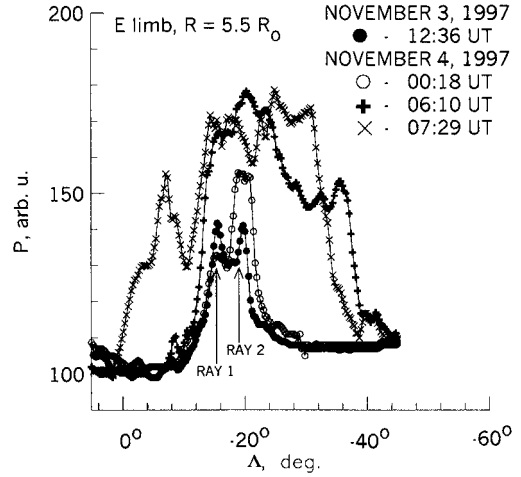

Figure 5. Brightness distribution $P(\Lambda)$ at different instants of time prior to and during the propagation of the CME along the streamer belt lying normal to the plane of the sky: ●, 3 November 1997 (12:36 UT); ○, 4 November 1997 (00:18 UT); +, 06:10 UT; ×, 07:29 UT. E limb. $R = 5.5\ R_\odot$.

Figure 4 shows the brightness distributions $P(\Lambda)$ at three different distances R at the E limb for 12:36 UT on 3 November 1997, prior to the production of the CME.

Two closely spaced rays are traceable at the three distances. Weak brightness maxima at $\Lambda \approx -10°$ and at $\Lambda \approx (-24$ and $-26)°$ are within the error of measurement, and they are difficult to identify with rays. (An analysis of the data from the C3 instrument permits them to be traced to distances 20–30 $R_\odot$). The time variation of the distribution $P(\Lambda)$ at $R = 5.5\ R_\odot$ prior to and during the passage

of the CME is shown in Figure 5. It is evident from the figure that during more than 12 hours prior to the production of the CME, starting from 12:36 UT on 3 November 1997, ray 2 increases its brightness and angular size, while ray 1 decreases its brightness. The enhancement of the brightness in ray 2 is associated with the arrival of additional plasma of increased density from the Sun, similar to the one detected earlier in Eselevich and Eselevich (2000a). In the region of the streamer top and below it, the enhancement of the brightness of rays 1 and 2 is observed as the process of 'uplift' and 'swelling' of the Helmet prior to the production of the CME. This phenomenon was, for the first time, pointed out by Illing and Hundhausen (1986). A further enhancement of the flow in ray 2 leads to an abrupt asymmetric angular expansion of its angular distribution $P(\Lambda)$ toward the side opposite to the location of ray 1 (see 06:10 UT on 4 November in Figure 5). Starting somewhat earlier than 06:10 UT (see Figure 5), the brightness increases in ray 1 as well, which ultimately leads to an asymmetric broadening of ray 1 toward the side opposite to ray 2 (see 07:29 UT). The peak at about -8 deg is not a ray because it is absent on the expanded $P(\Lambda)$-profiles within distances $R < 5\ R_\odot$ and $R > 6\ R_\odot$.

The two processes of asymmetric expansion of rays 1 and 2 result in a pattern of a more symmetric (with respect to the original location of the rays) brightness distribution $P(\Lambda)$ in the CME at 07:29 UT. The typical angular size of this distribution is $d \approx 35°$. Assuming the angular size $d_0 = 3°$ for each of the rays, for $n = 2$ we obtain $D \approx 14°$ in accordance with formula (1). The time delay of the asymmetric expansions of rays 1 and 2 reflects the independence of the propagation of additional plasma from the Sun in these rays. This is supported by Figure 6 (upper and bottom panels). The panels in this figure show the distributions $P(R)$ at different times for two angles: $\Lambda \approx -7°$ and $\Lambda \approx -35°$. The former of these angles corresponds to the flow propagating in the region of expanded ray 1, and the latter corresponds to the flow propagating in the region of expanded ray 2.

In Figure 6, the amplitude of the front h within distances $R > 15\ R_\odot$ is measured from the line A which represents the $\Delta P/P \leq 5\%$ dependence averaged over random spatial oscillations with a relative amplitude $\overline{P(R)}$. Large crosses correspond, at $h = h/2$, to the middle points of traveling fronts of these flows. It is evident from Figure 6, for example, that at 11:50 UT the front of the flow traveling at the angle $\Lambda \approx -35°$ is at $R \approx 24\ R_\odot$, whereas the front of the flow toward $\Lambda \approx -7°$ reaches only the distance $R \approx 19\ R_\odot$. The respective fronts in Figure 6 are shown by pairs of intersecting straight lines. Figure 7 gives the $V(R)$ profile of the flow fronts in each of these directions. It can be seen that they differ markedly for $R < 20\ R_\odot$, but the difference between the two profiles decreases at greater distances and both flows eventually merge into a single one for $R > 20\ R_\odot$, and form a common CME flow.

The described behavior of the additional plasma from the Sun in neighboring brightness rays of the streamer belt prior to and during the passage of the CME were observed in the other three events mentioned above. For each of them, $V(R)$

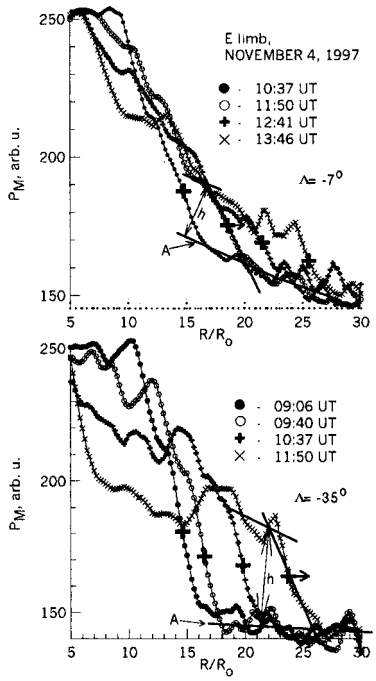

Figure 6. Brightness distribution P as function of the distance R from the Sun's center in the case of the CME propagating along the streamer belt lying normal to the plane of the sky, at successive times on 4 November 1997, for two values of the apparent latitude (within the angular opening of the CME): *upper panel* – $\Lambda = -7°$ (●, 10:37 UT; ○, 11:50 UT; +, 12:41 UT; ×, 13:46 UT); *bottom panel* – $\Lambda = -35°$ (●, 09:06 UT; ○, 09:40 UT; +, 10:37 UT; ×, 11:50 UT.) E limb.

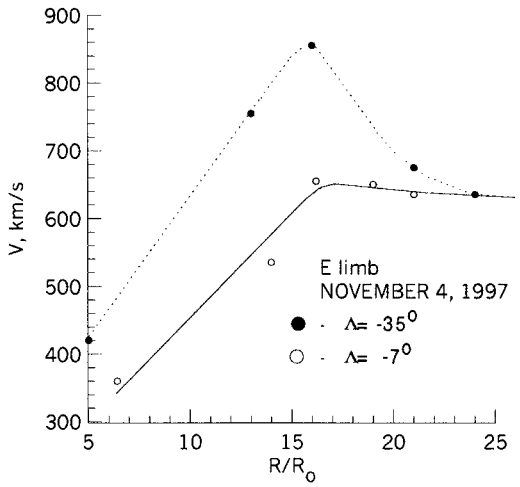

Figure 7. The velocity V of the plasma front versus distance R for two angles within the angular opening of the CME: ●, $\Lambda = -35°$; ○, $\Lambda = -7°$. The streamer belt is normal to the plane of the sky. E limb. 4 November 1997.

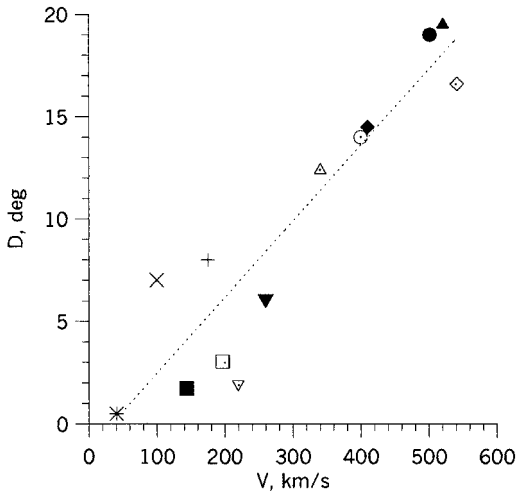

Figure 8. The increase of D (see formula (1)) of the angular size of the brightness ray versus velocity V of the plasma propagating along it, of the type: $*$, □, front of the plasma occupying the ray (slow solar wind); ■, $\times$, and ∇, blob; ▼, ●, ▲ and △, +, ○, ♦ and ◊ – CME.

was also measured and the mean value D of the increase of the angular size of a separate ray during the passage of the CME was determined.

4. Discussion

Our investigations have shown that the appearance of blobs and CMEs is almost always accompanied by additional anti-sunward plasma occupying the ray. A correlation between the process of occupation of the ray by additional plasma, on the one hand, and blobs and CMEs, on the other, is traceable in Figure 8. The figure shows the dependence of the increase of the angular size D of the ray on the plasma velocity V along the ray at a given distance $R = 6\ R_{\odot}$. This value of R was selected because at larger distances it is difficult to measure the velocity of additional plasma due to the strong transformation of its front (see Figure 2 in Eselevich and Eselevich, 2000a.) For the CME composed of several rays, D was evaluated from (1).

In these cases, as the accurate number of expanding rays was unknown, the error of determining D was the largest, $\approx \pm 15\%$

It is evident from Figure 8 that the lowest velocities and, accordingly, the smallest D correspond to rays occupied by additional plasma (the symbols $*$ and □ in Figure 8), while blobs are comparable or on average have larger velocities and larger D (the symbols ∇, $\times$, ■). Still larger values of V and D correspond to the CME. Furthermore, the values of D obtained from the measured angular size of the CME in the plane of the streamer belt (the symbols ▼, ▲, ♦ and ◊ in Figure 8)

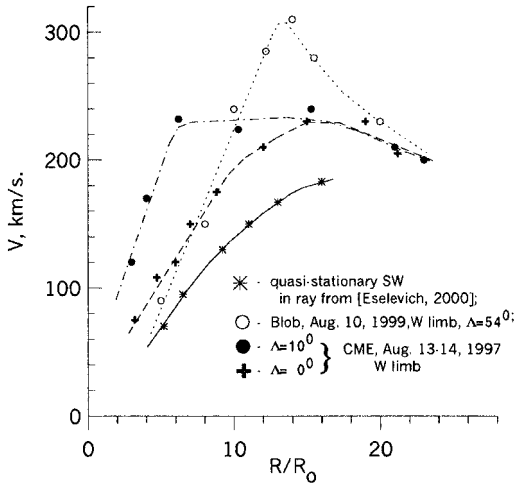

Figure 9. Velocity dependencies $V(R)$ for different types of plasma flow along the ray of the streamer belt or along a particular angle Λ: $*$, quasi-stationary solar wind along the brightness ray from Paper 1; ○, blob, 10 August 1999, W limb, $\Lambda = 54°$; ● ($\Lambda = 10°$), and + ($\Lambda = 0°$ – CME, 13–14 August 1997, W limb).

and in a plane normal to the plane of the streamers (the symbols ○ and ●, +, △ in Figure 8) for a given V turned out to be similar.

Because of the limited number of events in Figure 8, one cannot say with confidence whether or not the velocities of the fastest blobs can coincide with those of the slowest CMEs having minimum values of D. However, our investigations of more than twenty events showed that at $R = 20\ R_\odot$ the velocities of the blobs are 200–400 km s^{-1}. This is consistent with the results presented in Figure 6 (upper and middle panels) from Sheeley *et al.* (1997). A comparison of the upper and middle panels with the bottom panel of Figure 6 reveals that the mean quasi-parabolic trajectory of $V(R)$ for the blobs passes through the lower area of the dots of the plot in Figure 6 (bottom panel). Thus it also follows from Sheeley *et al.* (1997) that the velocities of the blobs are similar to those of the slowest CMEs.

Further evidence that the smallest CME and the largest blobs move at approximately the same speed is given in Figure 9 for distances greater than about 20 $R_\odot$. The figure presents the velocity dependencies $V(R)$ for three different types of plasma flow: $*$ - quasi-stationary SW in the brightness ray of the streamer belt from (Eselevich and Eselevich, 2000b); ○, blob in the ray of the streamer belt on 9–10 August 1999, ($\Lambda \approx 54°$, at the W limb, streamer belt in the plane of the sky); ● and +, CME on 13–14 August 1997 at the W limb, respectively, along the brightness rays at $\Lambda \approx 10°$ and $\Lambda \approx 0°$ (the streamer belt is perpendicular to the plane of the sky). It is evident from Figure 9 that within distances of up to 15 $R_\odot$, the CME is composed by composed by two rays, whose plasma propagates independently, and is differently accelerated until a common speed is reached, at about 15 $R_\odot$. One can see that the initial portion of the $V(R)$ profile of one of

these flows (●) resembles very much the corresponding profile of the blob (○), and the profile of the other flow (+) is like the profile of a quasi-stationary SW (∗). Possibly, a common mechanism is at work in all these events (with a different effectiveness, however).

In summarizing what has been presented above, we can state that the three types of flow under consideration – the process of occupation of the ray by an additional plasma, blobs, and CMEs are characterized by a common, linear dependence of D upon V (at $R = 6\ R_{\odot}$), Figure 8. The existence of such a dependence needs to be confirmed in a further analysis of a large number of events and suggests the following two important conclusions:

(1) The process of occupation of the ray by additional anti-sunward plasma of increased density and, as a consequence, the expansion of the ray constitute a common fundamental process during the production both of blobs and of CMEs. The difference between the blob and the CME seems to lie in the range of values of the characteristics considered above, namely: n, D, and V are, in most CMEs, larger than in blobs.

(2) Since the number of rays participating in the formation of a CME, in the plane of the streamer belt and in a plane normal to the belt, is different, hence the CME size $L_{\parallel}$ and $L_{\perp}$ in these two planes can differ, namely: $L_{\parallel} \geq L_{\perp}$.

The above considerations permit us to propose the following qualitative picture of the occurrence of blobs and CMEs. The source of energy for their production is provided by an additional anti-sunward directed plasma flow with increased density n, containing its own magnetic field B that is likely to exceed the mean magnetic field B_0 of the brightness ray (of the magnetic tube) which it occupies. If $nkT + B^2/8\pi \gg B_0^2/8\pi$, then the angular size of the tube (ray) will increase. The higher the pressure of the plasma entering the tube, the larger is the size d to which the tube 'swells' and the nearer to the solar surface is the level at which this 'swelling' can start. The mechanism responsible for the interaction of a high-pressure plasma flow with the magnetic tube leading to the formation of blobs and CMEs, seems to have an explosive character and still remains unclear.

5. Conclusions

(1) The generation of blobs and CMEs is commonly accompanied by the process of occupation of the ray (or rays) of the streamer belt by additional anti-sunward moving plasma of increased density.

(2) Blobs are similar, in their basic characteristics, to CMEs having a relatively small size and velocity.

(3) Generally the CME size in the plane of the streamer belt can exceed its size in the direction normal to the belt.

(4) The formation mechanism of CMEs and their energetics seem to be associated with the energy of additional plasma of increased density from the Sun which,

from time to time, occupies separate brightness rays of the streamer belt. This factor should be taken into consideration when constructing theoretical models of CMEs.

Acknowledgements

The SOHO/LASCO data used here are produced by a consortium of the Naval Research Laboratory (U.S.A.), Max-Planck-Institute fuer Aeronomie (Germany), Laboratoire d'Astronomie (France), and the University of Birmingham (U.K.). SOHO is a project of international cooperation between ESA and NASA. Wilcox Solar Observatory data used in this study were obtained via web site *http://quake.stanford.edu/wso* at 1998:05:14–18:43:35 PDT courtesy of J.T. Hoeksema. The Wilcox Solar Observatory is supported by NASA, NSF, and ONR. We are grateful to V. M. Mikhalkovsky for his assistance in preparing the English version of the manuscript. Grant governmental support for Russian Federation's leading scientific schools N961596733 and GNTP 'Astronomy'.

References

Eselevich, V. G. and Eselevich, M. V.: 1999, *Solar Phys.* **188**, 299.
Eselevich, V. G. and Eselevich, M. V.: 2000a, *Solar Phys.* **195**, 319.
Eselevich, V. G. and Eselevich, M. V.: 2000b, *Solar Phys.* **197**, 101.
Illing, R. M. E. and Hundhausen, A. J.: 1986, *J. Geophys. Res.* **91**, 951.
Sheeley, N. R. Jr., *et al.*: 1997, *Astrophys. J.* **484**, 472.
Wang, Y.-M. *et al.*: 1998, *Astrophys. J.* **498**, L165.
Wang, Y.-M., Sheeley, N. R. Jr., Howard, R. A., St.Cyr, O. C., and Simnett, G. M.: 1999a, *Geophys. Res. Let.* **26**, 1203.
Wang, Y.-M., Sheeley, N. R. Jr., Howard, R. A., Rich, N. B., and Lamy, P. L.: 1999b, *Geophys. Res. Let.* **26**, 1349.